Imaging DNA damage allows detection of preneoplasia in the BALB-neuT model of breast cancer.

B. Cornelissen,S. Able,C. Kartsonaki,V. Kersemans,P. D. Allen,F. Cavallo,J. Cazier,M. Iezzi,J. Knight,R. Muschel,S. Smart,K. A. Vallis
Imaging DNA damage allows detection of preneoplasia in the BALB-neuT model of breast cancer.
THE JOURNAL OF NUCLEAR MEDICINE (2014) 55
DOI: 10.2967/jnumed.114.142083

Imaging DNA Damage Allows Detection of Preneoplasia in the BALB-neuT Model of Breast Cancer

Bart Cornelissen[1], Sarah Able[1], Christiana Kartsonaki[1], Veerle Kersemans[1], P. Danny Allen[1], Federica Cavallo[3], Jean-Baptiste Cazier[1], Manuela Iezzi[2], James Knight[1], Ruth Muschel[1], Sean Smart[1], Katherine A. Vallis[1]

[1] CR-UK/MRC Oxford Institute for Radiation Oncology, Department of Oncology, Oxford University, Oxford, United Kingdom

[2] CeSI Foundation, University G. d' Annunzio, Chieti, Italy

[3] Molecular Biotechnology Center, University of Turin, Turin, Italy

Author to whom correspondence should be addressed:
Professor K. A. Vallis
CR-UK/MRC Gray Institute for Radiation Oncology and Biology,
University of Oxford,
Radiobiology Research Institute,
Churchill Hospital,
Oxford, OX3 7LE
Tel: +44 (0)1865 255850
Fax: +44 (0)1865 857533
Email: katherine.vallis@oncology.ox.ac.uk

Running Title: DNA Damage Imaging In Breast Cancer

Word count: 4975

ABSTRACT

A prominent feature of many human cancers is oncogene-driven activation of the DNA damage response (DDR) during early tumorigenesis. It has been shown previously that non-invasive imaging of γH2AX, a DNA damage signaling protein, is possible using ^{111}In-labeled anti-γH2AX antibody conjugated to the cell-penetrating peptide, TAT. The purpose of this study was to investigate whether ^{111}In-anti-γH2AX-TAT detects the DDR during mammary oncogenesis in BALB-neuT mice.

Methods: Mammary fat pads from BALB-neuT and wild-type mice (aged 40-106 days) were immunostained for γH2AX. ^{111}In-anti-γH2AX-TAT or a control probe was administered intravenously to BALB-neuT mice. Single-photon emission computed tomography (SPECT) was performed weekly and compared to tumor detection using palpation and DCE-MRI imaging.

Results: γH2AX expression was elevated in hyperplastic lesions in the mammary fat pads of BALB-neuT mice aged 76-106 days compared to normal fat pads from younger mice and carcinomas from older mice (13.5±1.2 γH2AX foci/cell versus 5.2±1.5 [P<0.05] and 3.4±1.1 [P<0.001], respectively). Serial SPECT imaging revealed a 2.5-fold increase in ^{111}In-anti-γH2AX-TAT accumulation in the mammary fat pads of mice aged 76-106 days, compared to control probe (P=0.01). The median time to detection of neoplastic lesions by ^{111}In-anti-γH2AX-TAT (defined as >5% injected dose per gram of tissue) was 96 days compared to 120 and 131 days for DCE-MRI and palpation, respectively (P<0.001).

Conclusion: DDR-imaging using ^{111}In-anti-γH2AX-TAT identified mammary tumors significantly earlier than MRI. Imaging the DDR holds promise for the detection of preneoplasia and as a technique for screening cancer-prone individuals.

Keywords: γH2AX; Molecular imaging; Balb-NeuT; Breast cancer; Early diagnosis

INTRODUCTION

The DNA damage response (DDR) is a highly regulated cellular process that follows exposure to ionizing radiation (IR) and other genotoxic insults (*1*). The DDR is activated during the earliest stages of cancer development, when it is triggered by the onset of oncogenic stress. Signaling via the ATM-Chk2-p53 DDR pathway minimizes genomic instability and inhibits cell cycle progression and tumor formation (*2*). This protective mechanism is eventually overridden, possibly precipitated by mutations of the p53 gene (*3*). Early reports of DDR activation during bladder, colon, breast, skin and lung cancer development showed that it was accompanied by the activation of signaling proteins downstream of pATM, including pChk2 and γH2AX (*4, 5*). DDR activation has since been observed to occur during the development of many other types of cancer including pancreatic (*6*), ovarian (*7*) and hepatocellular carcinomas (*8*). Given the near ubiquitous nature of DDR activation during oncogenesis, it has been suggested that markers of DNA replication stress and constitutive DDR activation might distinguish neoplastic growth from normal tissues. This has been substantiated by immunohistochemical analyses of human tissues. In one study markers of DDR activation were observed only in sub-populations of lymphocytic cells in bone marrow, spermatocytes in adult testes and basal esophageal cells (*4*). This raises the possibility that detection of DDR activation in vivo could allow early detection of precancerous and cancerous lesions (*9*).

It has been shown previously that an anti-γH2AX antibody-based imaging probe can detect γH2AX non-invasively (*10*). Anti-γH2AX antibodies were modified by the addition of the HIV-1 transactivator of transcription protein-derived cell-penetrating peptide, TAT, which harbors a non-classical nuclear localization sequence, promoting nuclear translocation of the conjugate. Anti-γH2AX-TAT was radiolabeled with indium-111 (^{111}In), to allow SPECT imaging. Following induction of γH2AX by X-irradiation or bleomycin, ^{111}In-anti-γH2AX-TAT accumulated in human breast cancer xenografts in athymic mice, and the extent of ^{111}In uptake was linearly

dependent on the level of γH2AX expression (*10*).

In this report the ability of the ^{111}In-anti-γH2AX-TAT probe to detect DDR during tumorigenesis was investigated using a transgenic mouse model of breast cancer in which the mouse mammary tumor virus (MMTV) promoter drives neuT expression. NeuT, a variant of the rat neu HER2-homolog, contains a point mutation in the transmembrane region and is highly tumorigenic compared to wild-type (WT) neu or human HER2 (*11*). When BALB-neuT mice reach 21-28 days of age, the neuT protein is over-expressed in mammary glands and areas of atypical hyperplasia start to form (*12*). These progress to *in situ* carcinomas at about day 60 and to invasive cancers by day 120-150. Neoplastic change occurs, albeit asynchronously, in all mammary glands so that by about 120 days one or more tumors are palpable and by about day 230 (33 weeks) all 10 mammary glands contain palpable tumors (*13*). In this study we explored the ability of ^{111}In-anti-γH2AX-TAT SPECT imaging to detect tumors during oncogenesis in BALB-neuT mice.

MATERIALS AND METHODS

Animal Model

All animal procedures were carried out in accordance with the UK Animals (Scientific Procedures) Act 1986 and with local ethical committee approval. Female WT BALB/c mice (Charles River, Wilmington, MA, USA) were crossed with male BALB-neuT mice (gift from Guido Forni). The BALB-neuT strain originated from a transgenic CD1 random-bred breeder male mouse carrying the mutated rat *neuT* oncogene driven by the MMTV promoter (*1*). The mutated gene encodes a single point mutation that replaces the valine residue at position 664 in the transmembrane (TM) domain of p185/neu with glutamic acid. This mutation promotes p185 homo- and heterodimerization and transforms the *neu* protooncogene into a dominant transforming oncogene. Offspring of the BALB-neuT male and WT female cross were genotyped using the following primers: 5'-CGCACGTCCTCCAGGTAG-3' and 5'-GATTCCAACGACCACCACTA-3'. NeuT-positive female mice were used for experiments.

Immunohistochemistry

At selected time points, mammary tissue or mammary tumors were harvested from female BALB/c or BALB-neuT mice. Flash frozen tissues were embedded in OCT and 10 μm sections were prepared. Tissue sections were stained with haematoxylin/eosin and images were acquired using a wide-field microscope. Alternatively, sections were washed to remove OCT, fixed (4% PFA, 10 min, room temperature), permeabilized (1% triton X-100 in PBS, 10 min, room temperature), blocked (1% BSA in PBS, 1 h, 37 °C), and incubated with anti-γH2AX antibodies raised in mouse (Calbiochem, Millipore, Watford, UK; 1:800 in blocking buffer, 1 h, 37 °C), or with anti-pATM antibodies raised in rabbit (R&D Systems, Minneapolis, MN, USA), followed by AlexaFluor488(AF488)-labeled goat anti-mouse or AlexaFluor555(AF555)-labeled goat anti-rabbit antibody (Invitrogen, Paisley,UK; 1:250 in blocking buffer, 1 h, 37 °C). Sections

were mounted with Vectashield containing DAPI to stain DNA (Vector Laboratories, Peterborough, UK), and images were acquired using confocal microscopy (Zeiss 710; Carl Zeiss Ltd., Welwyn Garden City, UK). Enumeration of γH2AX foci was performed manually in >1500 cells per samples, on >10 randomly selected view fields.

In Vivo Imaging and Biodistribution

^{111}In-anti-γH2AX-TAT and the non-specific control probe, ^{111}In-rabbitIgG-TAT (^{111}In-rIgG-TAT), and the fluorophore-labeled probe, Cy3-anti-γH2AX-TAT, were synthesized as reported (*10*). SPECT and CT images of BALB-neuT mice aged between 43 and 145 days were acquired under isoflurane anesthesia using a small animal nanoSPECT/CT scanner (Bioscan, Washington DC), 24 h after i.v. administration of ^{111}In-anti-γH2AX-TAT (5 µg; 16 animals) or ^{111}In-rIgG-TAT (5 µg; 16 animals). Imaging was repeated weekly for part of the period between the ages of 43 and 145 days per animal (5 MBq ^{111}In per scan). Animals were euthanized when tumor size reached the permitted upper limit (12 mm gross median diameter). Volume of interest (VOI) analysis of mammary fat pads and selected normal tissues was performed using the Inveon Research Workplace package (Siemens, Camberley, UK). ^{111}In uptake in mammary fat pads and the age of animals were recorded. Tumors were scored as positive when the percentage of the injected dose per gram of tissue (%ID/g) exceeded 5%ID/g. ^{111}In-anti-γH2AX-TAT (5 µg) was administered i.v. to BALBc WT mice. Following acquisition of SPECT images at 24 h p.i., mice were euthanized and organs were removed, weighed, and counted for radioactivity. To demonstrate γH2AX targeting in vivo BALB-neuT or BALB/c WT mice aged 80 to 100 days (3 mice per group) received Cy3-anti-γH2AX-TAT (5 µg) or PBS intravenously (i.v.). At 24 h post-injection (p.i.), fluorescence imaging was performed, using an IVIS200 system (Perkin Elmer, Waltham, MA, USA), as described previously (*10*). Mammary fat pads were removed, flash frozen, sectioned and processed for γH2AX immunostaining.

MRI Imaging

T1-weighed and dynamic contrast enhanced MRI (DCE-MRI) imaging of BALB-neuT mice of different ages was performed before and 20 min after i.v. administration of Omniscan (15 µmol, 0.5 M gadodiamide; GE Healthcare, Amersham, UK), using a dedicated small-animal MRI. Data were collected using a T1-weighted, gradient and RF spoiled, respiration triggered, 3-D gradient-echo sequence on a Varian/Agilent 4.7T MRI camera (Agilent, Yarnton, UK). Imaging parameters were: flip angle = 10º; TR=2.06 ms; TE=0.93 ms; FOV=54 x 27 x 27 mm^3; isotropic 420 µm resolution; 11 s temporal resolution. After acquisition of 10 frames, 15 µmol Omniscan™ was injected intravenously over 5 s via a catheter placed in a tail vein. Images were acquired for a further 20 minutes. Semi-quantitative Gd-uptake parameters (area-under-the-curve (AUC), first uptake moment) on a voxel-per-voxel basis were extracted for the whole tumour using Matlab, and parametric images generated. Images were inspected, and where tumors larger than 3x3 voxels was found, mice were scored as positive.

Statistical Methods

All data and graphs are expressed as mean ± one standard deviation, unless defined otherwise. Differences in the number of γH2AX foci/cell were assessed using an ANOVA test. Differences in the uptake of ^{111}In-anti-γH2AX-TAT and ^{111}In-rIgG-TAT were assessed by fitting a multilevel linear model with age, compound and set (data were obtained in two independent sets of n = 20 and n = 12) as explanatory variables. An interaction between age and compound was fitted to allow different effects of age for each compound. The uptake of ^{111}In-anti-γH2AX-TAT and ^{111}In-rIgG-TAT in mice of each age group was compared by fitting a multilevel linear model. Age groups were chosen based on known timing of development of mammary fat pad lesions in the BALB-neuT model. As a sensitivity analysis, 'nil' measurements, where no VOI could be drawn, since no signal/structure was discernable, were excluded and the models were fitted again, but this variation did not alter the conclusion. Times to tumor detection by SPECT, MRI

and palpation were compared using log-rank tests. All statistical analyses were performed using the statistical software package R (*14*).

RESULTS

DDR Activation During Carcinogenesis in BALB-neuT Mice

Histological examination of mammary fat pads from BALB-neuT mice confirmed the progressive development of atypical hyperplasia and in situ lesions, leading to invasive carcinoma by the age of 100-130 days (Fig. 1A). Normal duct structure was observed in mammary fat pads of mice aged up to 40 days. By 75 days changes of atypical hyperplasia were noted consisting of dilated, irregular ducts with pleomorphic cells containing enlarged nuclei. At 90-95 days there was extensive atypical hyperplasia with in situ carcinoma, typified by thickened ductal walls and small intra-ductal masses. Invasive carcinomas were apparent at 100-130 days (solid masses). In contrast, mammary fat pads from WT BALB/c mice aged 130 days showed normal histology (Supplementary Fig. S1A and S1B). DDR activation, as indicated by the phosphorylation of H2AX to form γH2AX, was observed in hyperplastic lesions and DCIS-like mammary fat pad lesions in BALB-neuT mice at 75 to 95 days (Fig. 1A). Also, although staining for total ATM in mammary fat pads/tumors was positive, with low-level expression at all time points tested, the activated form (pATM) of the enzyme was only clearly present at 75-95 days, further evidence of up-regulation of the DDR during this phase. The number of γH2AX foci was greater in hyperplastic lesions in mammary fat pads from mice aged 76-106 days than in mammary fat pads from mice aged <75 days (13.5±1.2 versus 5.2±1.5 foci/cell; $P<0.05$), and in carcinomas from mice aged >106 days (13.5±1.2 versus 3.4±1.1 foci/cell; $P<0.001$) (Fig. 1B).

Targeting γH2AX In Vivo

To confirm that systemically delivered anti-γH2AX-TAT probe co-localizes with γH2AX in vivo, fluorescence imaging of BALB-neuT or WT BALB/c mice (aged 80-100 days) was performed 24 h after i.v. administration of Cy3-anti-γH2AX-TAT. The fluorescent signal localized in mammary fat pads in BALB-neuT mice (Fig. 2A). No fluorescent signal was observed in fat pads of BALB/c mice or in BALB-neuT mice that received PBS i.v. A feature of

the BALB-neuT model is the development of lymph node metastases. Also, while the neuT oncogene is mainly expressed in mammary glands, it is expressed to a lesser extent in salivary glands. Therefore some of the areas of uptake may represent lymph node or salivary gland deposits. Mammary tissue was harvested and immunostained for γH2AX. Co-localization of Cy3-anti-γH2AX-TAT (red) and γH2AX foci (green) was observed (Fig. 2B).

^{111}In-anti-γH2AX-TAT SPECT Imaging

To study γH2AX expression, as a marker of DDR activation, throughout the progression of mammary fat pad lesions, BALB-neuT mice were imaged weekly using SPECT, 24 h after administration of ^{111}In-anti-γH2AX-TAT i.v. The data consist of 148 observations on 32 animals, obtained in 2 sets of n=20 and n=12 (Fig. 3A-C). Restriction on the number of weekly scans each animal underwent meant that no single animal was imaged throughout the entire period of interest (from 40-130 days). However, a complete time course that includes measurements from all mice is presented (Fig. 3C). Plots for individual animals for which at least 4 observations were made are shown in Supplementary Fig. S2. The uptake of ^{111}In-anti-γH2AX-TAT was higher than that of ^{111}In-rIgG-TAT (P=0.0038; adjusted for age and set). Intratumoral accumulation of both ^{111}In-anti-γH2AX-TAT and ^{111}In-rIgG-TAT was high in older mice (>106 days), compared to younger mice. This suggests that non-specific enhanced permeability and retention (EPR)-mediated uptake of IgG-TAT constructs occurs in mature tumors. This may be attributable to leakiness of vessels in large, fully established tumors. In mice aged less than 76 days, tumor uptake of ^{111}In-anti-γH2AX-TAT and ^{111}In-rIgG-TAT did not differ significantly (2.52±2.02 versus 1.42±1.72 %ID/g, respectively). This was consistent with the multilevel model in which the coefficient for ^{111}In-anti-γH2AX-TAT was estimated to be 1.19±0.92, P=0.24. That is, for the ^{111}In-anti-γH2AX-TAT group the uptake for ages <76 days is expected to be 1.19 higher than in the ^{111}In-rIgG-TAT group. However, ^{111}In-anti-γH2AX-TAT accumulated to a greater extent than ^{111}In-rIgG-TAT in the mammary fad pads of mice aged 76-106 days (3.67±3.01 versus 1.48±1.86 %ID/g, respectively; intercept 1.60±0.59 and beta for ^{111}In-anti-γH2AX-TAT 2.22±0.80; P=0.01 for

beta), which corresponds to the development of in situ and early invasive carcinomas. For this group ^{111}In-anti-γH2AX-TAT uptake often exceeded 5%ID/g, whereas in only one case did the uptake of the control probe marginally exceed 5%ID/g. Additionally, analysis of data on individual lesions showed that all lesions that became palpable during the study had been identified by SPECT imaging before becoming detectable by palpation. In 14 out of 16 mice, the first lesion to be detected by ^{111}In-anti-γH2AX-TAT SPECT imaging was subsequently also the first lesion to become palpable.

^{111}In-anti-γH2AX-TAT was administered to young or old BALB/c WT mice and following acquisition of SPECT images performed at 24 h followed by retrieval of tissues for radioactivity counting (Supplementary Fig. S3). Uptake of ^{111}In-anti-γH2AX-TAT was slightly higher in the mammary fat pads of young versus old mice: however, this did not reach statistical significance (mean +/- SD: 2.28±0.35 versus 1.21±0.49; P=0.10). The level of uptake in the mammary fat pads in BALB/c WT mice was therefore well below the 5%ID/g cut-off that was used to denote positive ^{111}In-anti-γH2AX-TAT uptake in BALB-neuT mice.

Lack of Effect of ^{111}In-RICs on γH2AX Expression and Tumor Growth

To evaluate the possibility that administration of ^{111}In-anti-γH2AX-TAT or ^{111}In-rIgG-TAT could itself affect tumor development, the tumor-free survival of mice that had undergone repeated imaging was compared to that of control animals. No significant differences were detected (log rank test; P=0.41) (Fig. 4). Similarly, in a group of animals aged 89-96 days there was no statistical difference in the number of γH2AX foci/tumor cell in mice that received ^{111}In-anti-γH2AX-TAT compared to those that did not. The mean γH2AX foci/cell 24 h after a single i.v. injection of ^{111}In-anti-γH2AX-TAT was 14.7±3.1 (n=12) versus 13.5±2.9 (n=6) for controls (P=0.65).

Early Detection of Precancerous Lesions

Small tumors were not identified in CT images, acquired to provide an anatomical

reference for SPECT images (results not shown). However, tumors with a diameter as small as 1.26 mm were visualized using T1-weighed MRI images and were particularly clearly identifiable in AUC-parameter maps generated after DCE-MRI (Fig. 5A). The median age at which tumors were detectable by DCE-MRI and palpation was 120 and 131 days, respectively (P=0.10). SPECT imaging using ^{111}In-anti-γH2AX-TAT was superior to DCE-MRI (P=0.058), with median age at detection of first tumor of 96 days (Fig. 5B).

DISCUSSION

Oncogenic stimulation leading to DNA replication stress occurs early in the development of cancer. The resulting accumulation of DNA damage triggers constitutive activation of the DDR, typified by expression of phosphorylated forms of key DNA repair proteins including pATM (S1981), γH2AX (S139) and pChk2 (Thr68) (*3, 5, 9, 15, 16*). As a result of DDR activation, DNA damage is repaired and its detrimental effects, including genomic instability, avoided. However, unrelieved oncogenic stress eventually results in a breach of this protective mechanism with subsequent progression to the malignant phenotype. A large body of published evidence has shown that DDR is activated during development of many tumor types (*17*). Several reports have shown immunohistochemical evidence that DDR proteins are highly expressed in precancerous lesions but less so in invasive cancers or corresponding normal tissues *(4-8)*. It is therefore logical to explore these molecules as biomarkers of early cancer development and reasonable to hypothesize that visualization of components of the DDR might provide an excellent means of early cancer detection (*9*). It was shown previously that it is possible to image DNA damage using the prototypic SPECT imaging tracer, ^{111}In-anti-γH2AX-TAT (*10*). We have used the same probe to test the hypothesis that DDR imaging can detect premalignant lesions in the BALB-neuT breast cancer model.

Expression of γH2AX was significantly increased in hyperplastic and DCIS lesions in mice aged between 76 and 106 days compared to normal mammary fat pads (from young mice) and mature tumors (from older mice) (Fig. 1B). pATM, the kinase primarily responsible for H2AX phosphorylation to form γH2AX, was also upregulated during this period, while total ATM remained unchanged. In contrast to this robust activation of the DDR in BALB-neuT-associated preneoplastic lesions, Reddy et al. found that the DDR was either weak or absent in hyperplastic lesions arising in some other transgenic mouse models of breast cancer. For example, only modest induction of γH2AX was observed in mammary lesions from MMTV-ErbB2 transgenic animals (*18*). One possible explanation for this difference is that NeuT is more potently oncogenic than erbB2 (*11*), and so is more likely to cause DDR activation. Interestingly,

a somatic model of breast carcinogenesis, consisting of intraductal injection of the avian retrovirus RCAS carrying Erbb2 in MMTV-*tva* mice, was associated with marked stimulation of the DDR (*18*).

Immunofluorescence staining for γH2AX in tumors from mice that had received Cy3-anti-γH2AX-TAT i.v. showed good co-localization of Cy3 with γH2AX foci; indicating that systemically administered antibody tracer is capable of penetrating tumor, internalizing into cancer cells and associating with its intranuclear target. Serial SPECT imaging using ^{111}In-anti-γH2AX-TAT in BALB-neuT mice showed that the γH2AX signal was greater in mammary fat pads of mice aged between 76 and 106 days, compared to animals in younger and older age groups. This was consistent with *ex vivo* immunostaining of mammary fat pads that revealed that γH2AX expression was highest in 76-106 day old mice.

It was important to investigate whether ^{111}In-anti-γH2AX-TAT itself increases DNA DSBs and, therefore, impairment of DNA repair, either through radiation dose deposition or by blocking signaling downstream of H2AX. However, we saw no evidence that ^{111}In-anti-γH2AX-TAT perturbs the system it is designed to image. Specifically, the number of γH2AX foci in tumor cells was unaffected by exposure to the probe and repeated administration of ^{111}In-anti-γH2AX-TAT or ^{111}In-rIgG-TAT had no effect on tumor-free survival of animals (Fig. 4).

^{111}In-anti-γH2AX-TAT SPECT imaging of the DDR was superior to anatomical imaging methods. CT, acquired as anatomical reference during SPECT, provided images with poor soft-tissue contrast such that only tumors >5 mm in diameter were detectable. T1-weighed MRI imaging and DCE-MRI imaging provided better contrast. However, the average age of mice when tumors first became detectable by DCE-MRI was 120 days, significantly later than detection by DDR-imaging using SPECT i.e. 96 days.

The data presented in Figure 3, show that uptake of both ^{111}In-anti-γH2AX-TAT and the non-specific probe is higher in carcinomas in older mice compared to intermediate-aged mice. This raises the question as to how the extent of uptake of ^{111}In-anti-γH2AX-TAT could be interpreted in a practical setting. Since SPECT imaging is

routinely combined with an anatomical imaging modality such as CT or MRI it is predicted that larger, late-stage lesions (i.e. the human equivalent of the mature cancers seen in mice > 106 days old) would be detected by correlative anatomical imaging. However, earlier stage lesions would be predicted to be positive for ^{111}In-anti-γH2AX-TAT uptake but lack CT/MRI evidence of a mass lesion. Thus it may be possible to distinguish between early and late stage lesions.

These results provide proof-of-principle that it is possible to image γH2AX non-invasively in preneoplastic lesions. However, further optimization of ^{111}In-anti-γH2AX-TAT is needed, since the ratio of tumor to normal tissue contrast achieved in SPECT images was modest. Investigation of other tumor models is needed to explore the generalizability of these findings. Further work is also required to determine whether all lesions with constitutive DDR activation are destined to become invasive cancers, as this is likely to be a significant determinant of the utility of this imaging approach. It is possible that the DDR is particularly prominent in senescent premalignant cells, which may or may not progress beyond metaplasia, since the DDR itself acts as a barrier to tumorigenesis (*19*). Imaging γH2AX provides no information about other modifications of H2AX, such as ubiquitination and sumoylation, that may also follow genotoxic insults and be functionally important.

A concerted effort is being made to develop imaging biomarkers for detection of preneoplasia in human cancers. The application of advanced endoscopic techniques to the diagnosis of premalignant lesions of the upper aerodigestive tract, bladder, colon, esophagus and bronchi is a major focus of research (*20, 21*). For example, confocal laser endomicroscopy (CLE) has recently been confirmed to significantly improve the identification of dysplasia in Barrett's esophagus when combined with high-definition white light endoscopy (HD-WLE) (*22*). Optical and fluorescence endoscopic imaging techniques hold promise as accurate methods for distinguishing preneoplastic from invasive lesions, but visualization is limited to a depth of a few mm or less and so they are not suitable for the diagnosis of endoscopically inaccessible or deep-seated lesions. Increasingly, the merits of functional MRI imaging for the

detection and characterization of precancerous lesions in the breast are being explored. For example, diffusion-weighted imaging helped differentiate high-risk breast lesions requiring further investigation from benign lesions (*23*). However, the specificity of these methods is not yet sufficient for widespread adoption in the clinic and further research is required to develop clinically robust imaging systems for the detection of breast preneoplasia.

The approach of DNA damage imaging has potential applications in the early detection of cancer and screening cancer-prone individuals (such as those with hereditary non-polyposis colorectal carcinoma, BRCA2 mutations and Peutz-Jeghers syndrome). Also the ability to image the DDR non-invasively would enable the response to DDR-targeted drugs to be monitored and might be useful in the development of cancer prevention strategies. Also, because DDR activation is a common phenomenon during tumorigenesis, γH2AX-targeted molecular imaging may be applicable to early detection of several types of cancer.

CONCLUSION

DDR-imaging using ^{111}In-anti-γH2AX-TAT identified mammary tumors significantly earlier than MRI. Imaging the DDR holds promise for the detection of preneoplasia and as a technique for screening cancer-prone individuals.

GRANT SUPPORT

This work was supported by the Medical Research Council, Cancer Research UK and by the Cancer Research UK/Engineering and Physical Sciences Research Council Oxford Cancer Imaging Centre.

FIGURE LEGENDS

Figure 1: Mammary fat pads, or mammary fat pad tumors were harvested from BALB-neuT mice of various ages. (A) Tissues were frozen, sectioned and stained with haematoxylin/eosin, or immunostained for γH2AX, pATM or ATM. Representative images are shown (scale bar = 10 μm). (B) The number of γH2AX foci per cell in harvested tissues was counted (one outlier depicted in grey), * $P<0.05$.

Figure 2: (A) Groups of 3 BALB-neuT or BALB/c WT mice aged 76-106 days received Cy3-anti-γH2AX-TAT or PBS i.v. Fluorescence images were acquired at 24 h p.i. (B) Mammary fat pads were removed, frozen, sectioned and stained for γH2AX, and counterstained with DAPI to visualize the nucleus (blue). Colocalization of γH2AX (green) and Cy3-anti-γH2AX-TAT (red) is observed (scale bar = 10 μm).

Figure 3: BALB-neuT mice of different ages received ^{111}In-anti-γH2AX-TAT or ^{111}In-rIgG-TAT i.v. at weekly intervals for up to 5 weeks. SPECT images were acquired 24 h p.i. (A) Maximum intensity projections (MIP) of representative animals. White circles denote areas of tumor development. (B) The uptake of ^{111}In in mammary tissue was quantified by VOI analysis. For ^{111}In-anti-γH2AX-TAT or ^{111}In-rIgGTAT observations were assigned to three groups by age and then within each age group the average observation for each mouse was calculated. The height of each bar represents the mean of these averaged observations and the error bars are +/- the standard error of the mean, * $P<0.05$. (C) As in (B), but without age-stratification of results.

Figure 4: Kaplan-Meier plot comparing tumor-free survival of control BALB-neuT mice (that did not receive imaging probes) to that of mice that were imaged on multiple occasions using ^{111}In-anti-γH2AX-TAT or ^{111}In-rIgG-TAT.

Figure 5: (A) T1-weighed images of BALB-neuT mice of varying ages were acquired on a 4.7 T MRI scanner. DCE-MRI: Repeated T1-weighed images were acquired after injection of gadodiamide, and the integrated signal enhancement (area under the curve; AUC) was calculated on a pixel-per-pixel basis. (B) Kaplan-Meier plot comparing the time to detection of precancerous lesions and tumors through palpation, DCE-MRI, all SPECT imaging (^{111}In-anti-γH2AX-TAT or ^{111}In-rIgG-TAT) and ^{111}In-anti-γH2AX-TAT SPECT designated as positive when the uptake of ^{111}In-anti-γH2AX-TAT $\geq$ 5 %ID/g.

REFERENCES

1. Thompson LH. Recognition, signaling, and repair of DNA double-strand breaks produced by ionizing radiation in mammalian cells: the molecular choreography. *Mutation Res.* 2012;751:158-246.
2. Li X, Xu H, Xu C, et al. The yin-yang of DNA damage response: roles in tumorigenesis and cellular senescence. *Int J Mol Sci.* 2013;14:2431-2448.
3. Bartkova J, Rezaei N, Liontos M, et al. Oncogene-induced senescence is part of the tumorigenesis barrier imposed by DNA damage checkpoints. *Nature.* 2006;444:633-637.
4. Bartkova J, Bakkenist CJ, Rajpert-De Meyts E, et al. ATM activation in normal human tissues and testicular cancer. *Cell Cycle.* 2005;4:838-845.
5. Gorgoulis VG, Vassiliou LV, Karakaidos P, et al. Activation of the DNA damage checkpoint and genomic instability in human precancerous lesions. *Nature.* 2005;434:907-913.
6. Koorstra JB, Hong SM, Shi C, et al. Widespread activation of the DNA damage response in human pancreatic intraepithelial neoplasia. *Mod Pathol.* 2009;22:1439-1445.
7. Kshirsagar M, Jiang W, Shih Ie M. DNA damage response is prominent in ovarian high-grade serous carcinomas, especially those with Rsf-1 (HBXAP) overexpression. *J Oncol.* 2012;2012:621685.
8. Matsuda Y, Wakai T, Kubota M, et al. DNA damage sensor gamma-H2AX is increased in preneoplastic lesions of hepatocellular carcinoma. *The Scientific World Journal.* 2013;2013:597095.
9. Halazonetis TD, Gorgoulis VG, Bartek J. An oncogene-induced DNA damage model for cancer development. *Science.* 2008;319:1352-1355.
10. Cornelissen B, Kersemans V, Darbar S, et al. Imaging DNA damage in vivo using gammaH2AX-targeted immunoconjugates. *Cancer Res.* 2011;71:4539-4549.
11. Quaglino E, Mastini C, Forni G, Cavallo F. ErbB2 transgenic mice: a tool for investigation of the immune prevention and treatment of mammary carcinomas. *Curr Protoc Immunol*. 2008; Chapter 20:Unit 20 9 1- 9-10.
12. Di Carlo E, Diodoro MG, Boggio K, et al. Analysis of mammary carcinoma onset and

progression in HER-2/neu oncogene transgenic mice reveals a lobular origin. *Lab Invest.* 1999;79:1261-1269.

13. Calogero RA, Cordero F, Forni G, Cavallo F. Inflammation and breast cancer. Inflammatory component of mammary carcinogenesis in ErbB2 transgenic mice. *Breast Can Res.* 2007;9:211.
14. R Core Team (2013). R: A language and environment for statistical computing. R Foundation for Statistical Computing, Vienna, Austria. URL http://www.R-project.org/.
15. Bartek J, Lukas J, Bartkova J. DNA damage response as an anti-cancer barrier: damage threshold and the concept of 'conditional haploinsufficiency'. *Cell Cycle.* 2007;6:2344-2347.
16. Bartek J, Bartkova J, Lukas J. DNA damage signalling guards against activated oncogenes and tumour progression. *Oncogene.* 2007;26:7773-7779.
17. Bartkova J, Horejsi Z, Koed K, et al. DNA damage response as a candidate anti-cancer barrier in early human tumorigenesis. *Nature.* 2005;434:864-870.
18. Reddy JP, Peddibhotla S, Bu W, et al. Defining the ATM-mediated barrier to tumorigenesis in somatic mammary cells following ErbB2 activation. *Proc Nat Acad Sci USA.* 2010;107:3728-3733.
19. Campisi J, d'Adda di Fagagna F. Cellular senescence: when bad things happen to good cells. *Nat Rev Mol Cell Biol*. 2007;8:729-740.
20. Vakoc BJ, Fukumura D, Jain RK, Bouma BE. Cancer imaging by optical coherence tomography: preclinical progress and clinical potential. Nature Rev Cancer. 2012;12:363-368.
21. Subramanian V, Ragunath K. Advanced endoscopic imaging: a review of commercially available technologies. *Clin Gastroenterol Hepatol*. 2014;12:368-376 e361.
22. Sharma P, Meining AR, Coron E, et al. Real-time increased detection of neoplastic tissue in Barrett's esophagus with probe-based confocal laser endomicroscopy: final results of an international multicenter, prospective, randomized, controlled trial. *Gastrointest Endosc.* 2011;74:465-472.
23. Parsian S, Rahbar H, Allison KH, et al. Nonmalignant breast lesions: ADCs of benign and high-risk subtypes assessed as false-positive at dynamic enhanced MR imaging. *Radiol.* 2012;265:696-706.

Figure 1

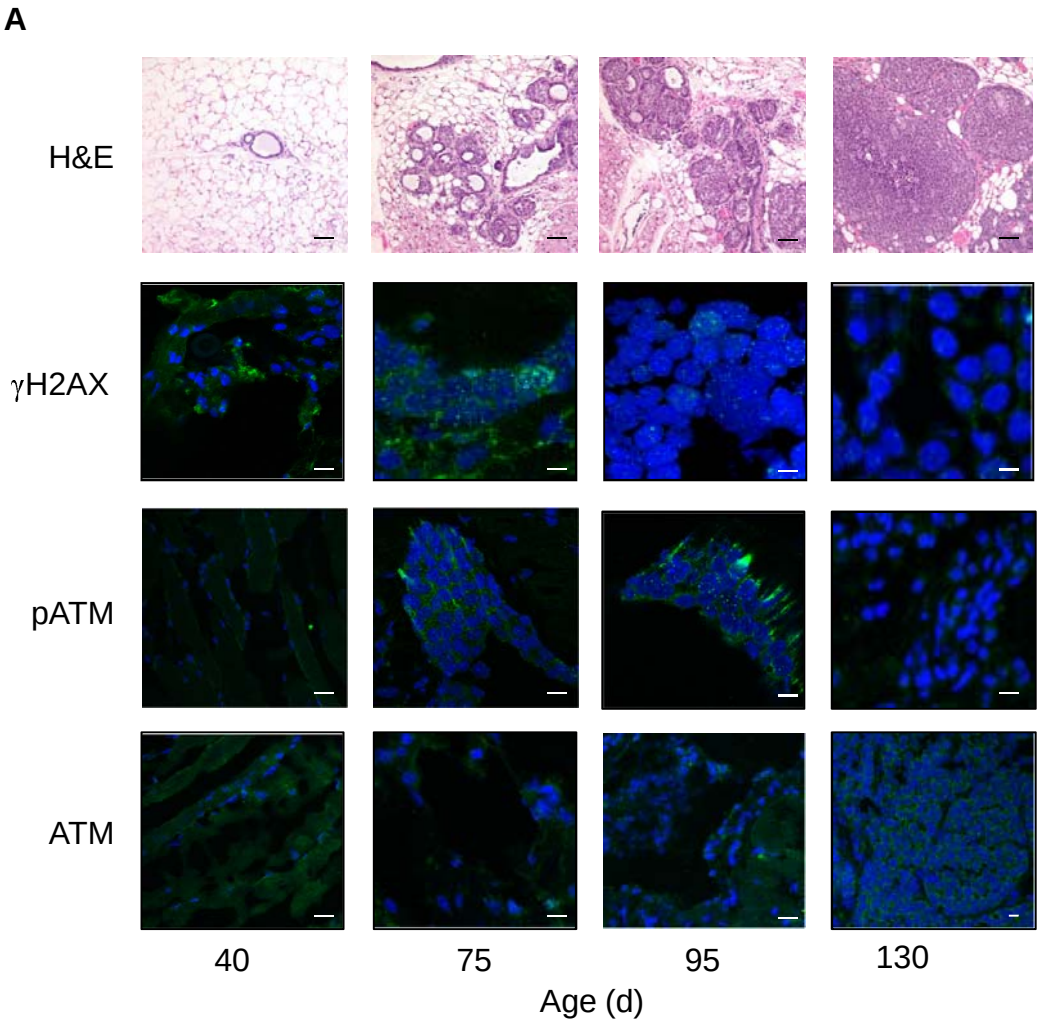
A
H&E
γH2AX
pATM
ATM
40
75
95
130
Age (d)

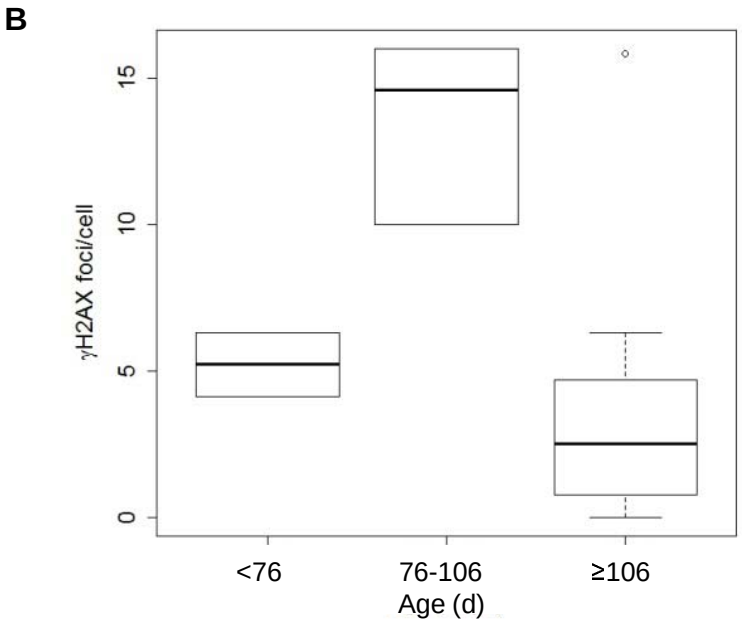
B
γH2AX foci/cell
0
5
10
15
<76
76-106
≥106
Age (d)

Figure 2

A

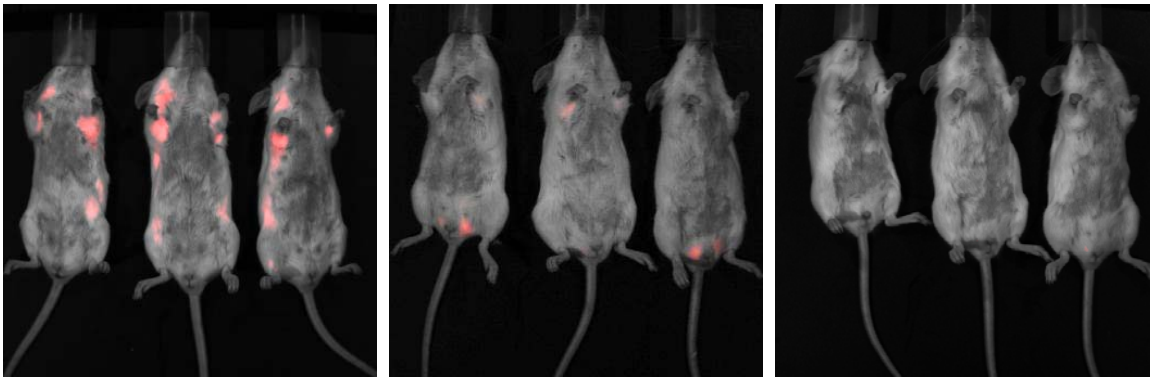

Cy3-anti-γH2AX-TAT
BALB-neuT mice

Cy3-anti-γH2AX-TAT
BALB/c WT

PBS
BALB-neuT

B

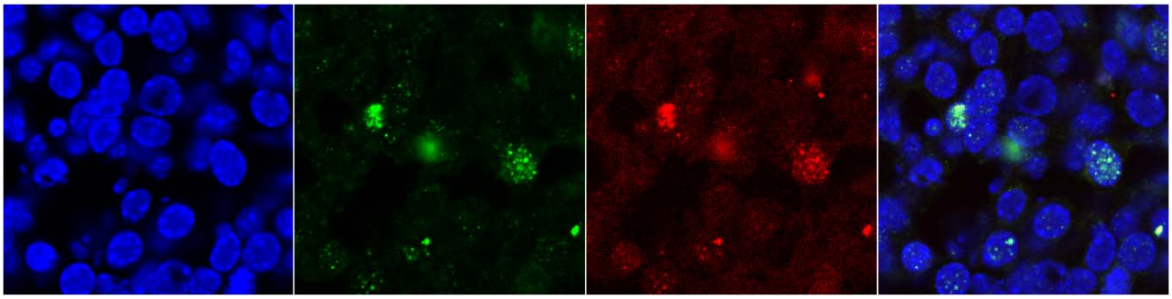

DAPI

γH2AX

Cy3-anti-
γH2AX-TAT

Merge

Figure 3

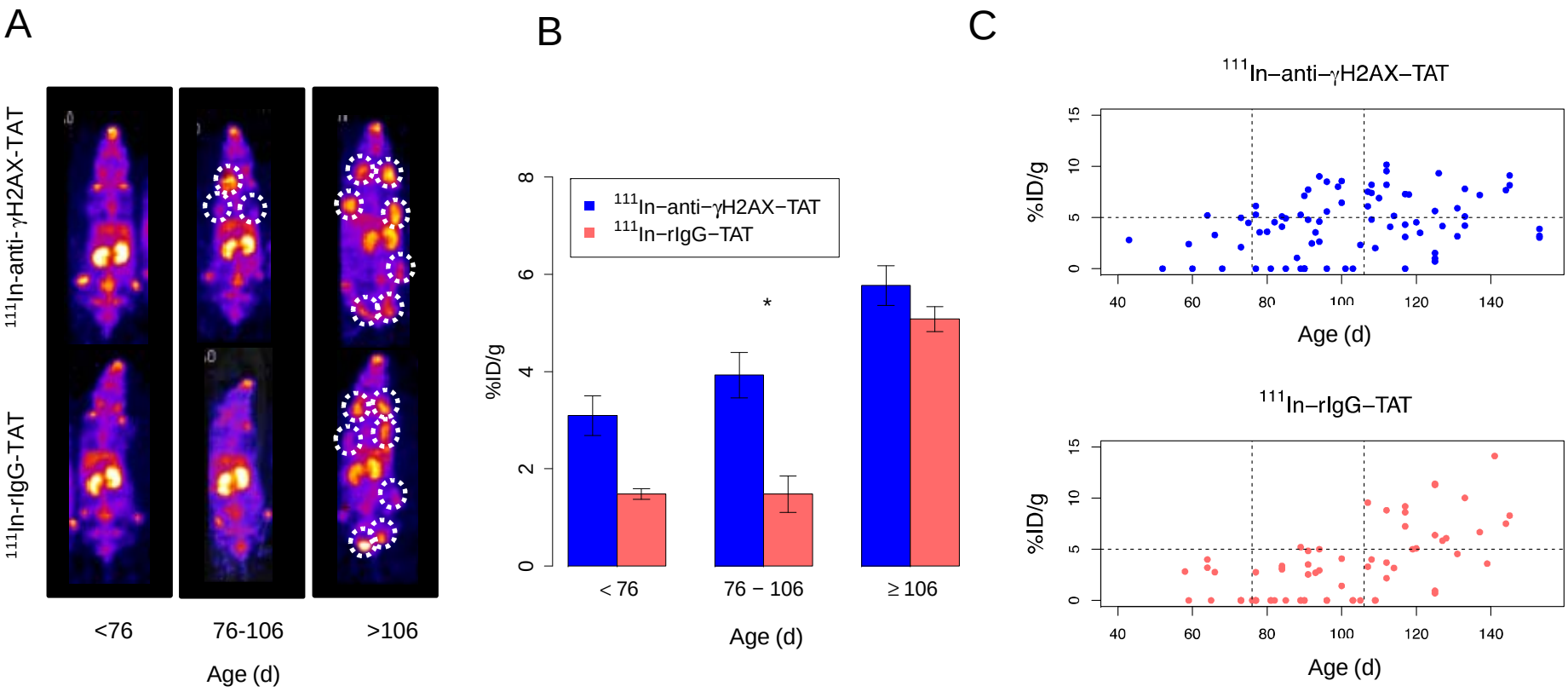
A
111In-anti-γH2AX-TAT
111In-rIgG-TAT
<76
76-106
>106
Age (d)
B
111In−anti−γH2AX−TAT
111In−rIgG−TAT
%ID/g
0
2
4
6
8
*
< 76
76 − 106
≥ 106
Age (d)
C
111In−anti−γH2AX−TAT
%ID/g
0
5
10
15
40
60
80
100
120
140
Age (d)
111In−rIgG−TAT
%ID/g
0
5
10
15
40
60
80
100
120
140
Age (d)

Figure 4

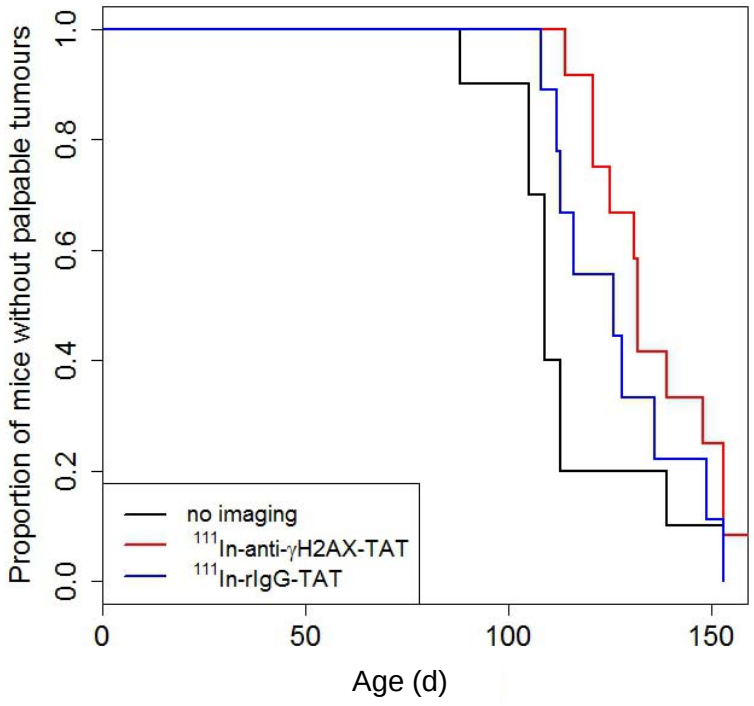
Proportion of mice without palpable tumours
0.0
0.2
0.4
0.6
0.8
1.0
0
50
100
150
Age (d)
no imaging
111In-anti-γH2AX-TAT
111In-rIgG-TAT

Figure 5

A

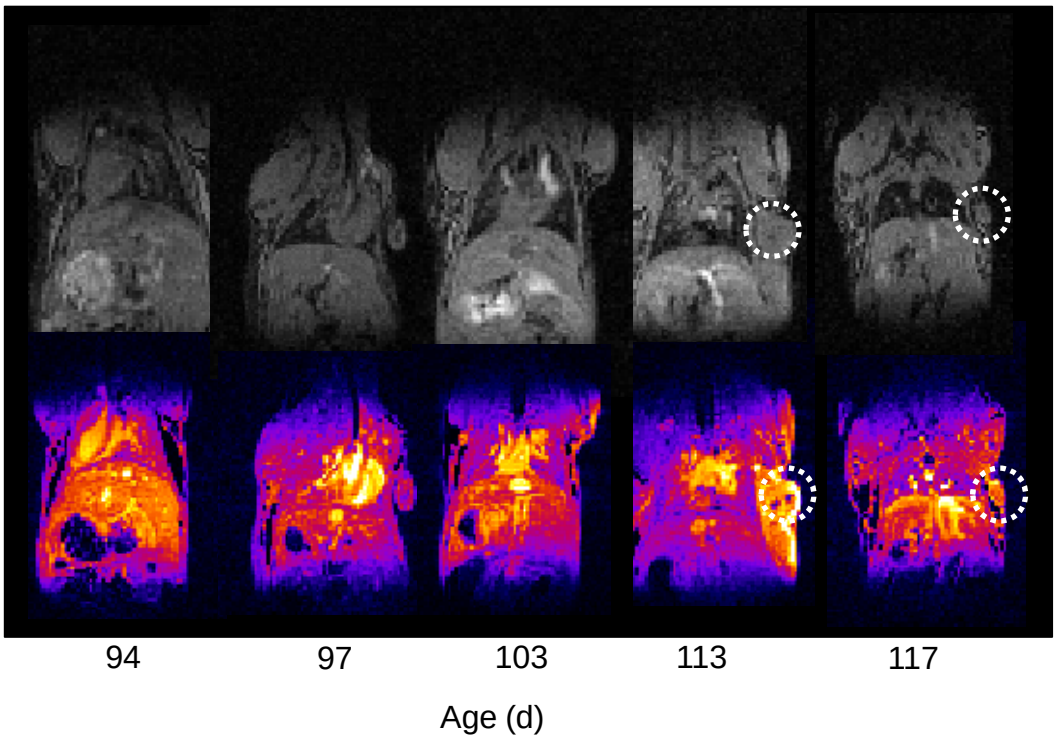
T1w
DCE
(AUC)
94
97
103
113
117
Age (d)

B

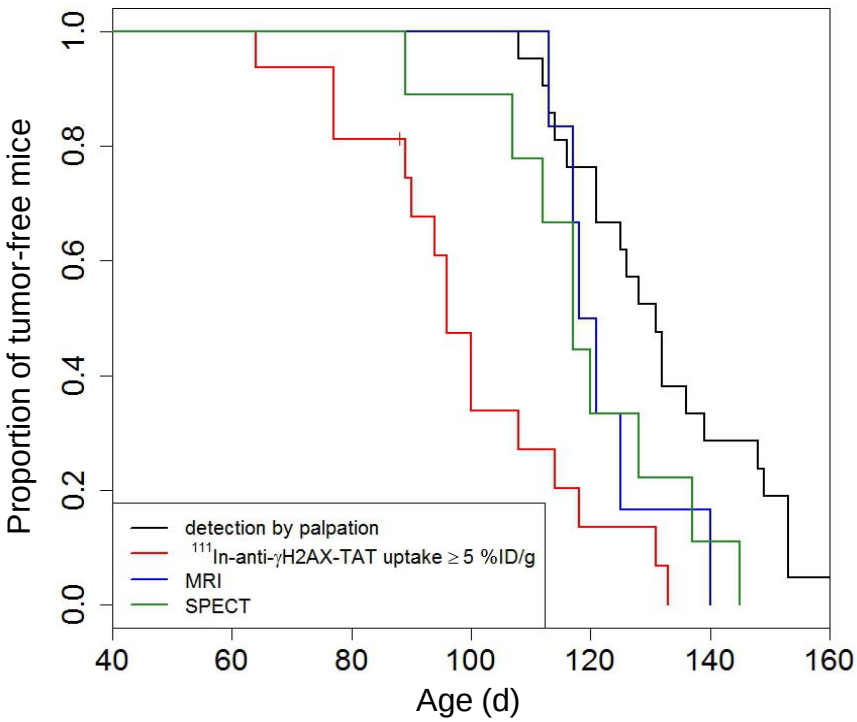
Proportion of tumor-free mice
0.0
0.2
0.4
0.6
0.8
1.0
40
60
80
100
120
140
160
Age (d)
detection by palpation
111In-anti-γH2AX-TAT uptake ≥ 5 %ID/g
MRI
SPECT